16TH EUROPEAN CONFERENCE ON EARTHQUAKE ENGINEERING THESSALONIKI 18 - 21 JUNE 2018

ESTIMATION OF QUALITY FACTOR (Q_B) AND SOURCE PARAMETERS USING ACCELEROGRAMS: NW-IRAN

Majid MAHOOD[1], Shima TAHERI[2]

ABSTRACT

High-frequency strong-motion data of two recent major earthquakes of the Ahar-Varzaghan of Northwestern Iran have been analyzed to determine the shear-wave quality factor for this region. Data from a local array of 12 stations, two main shocks (Ahar-Varzaghan doublet earthquakes of 11 August 2012 (Mw 6.4 and 6.2)), and 38 aftershocks were used to determine $Q_\beta(f)$ and the corresponding source parameters. By using the inversion algorithm in this study, an average relation in the form, $Q_\beta=(114\pm21)f^{(0.90\pm0.07)}$ is obtained for the Ahar-Varzaghan region of NW-Iran. The present inversion of strong-motion data gives the corner frequencies for these earthquakes as 0.18 and 0.15 Hz, respectively, which correspond to the stress-drop values of 87 bars and 38 bars, respectively. This $Q(f)$ relationship suggests a low Qo value and a high n value for high heterogeneous, tectonically and seismically active regions.

Keywords: Inversion; Attenuation; $Q_\beta(f)$; Ahar-Varzaghan Earthquake; Iran.

1. INTRODUCTION

Attenuation is a geophysical parameter that is sensitive to the lithology and physical properties like pressure, temperature, saturation with fluid, gas, etc. The value of attenuation in the crust, commonly described by the dimensionless quantity known as quality factor Q, shows a close relation with seismic activity. This parameter is used to measure the tendency of material to dissipate energy during deformations. The common idea considered Q as a ratio of potential energy to the dissipated energy over one period of harmonic deformations (Sato et al., 2012). The change in the Q values with time may be attributed to an increase of pressure in the crust producing new cracks and/or reopening of pre-existing cracks, which are the most viable mechanisms for increasing attenuation (Mahood, 2014). Recently, a technique has been developed by Joshi (2006a) which uses the S-phase of an accelerogram as input in an inversion algorithm and gives $Q_\beta(f)$ and corner frequency f_c of the input events. The approach suggested by Joshi (2006a) and subsequently modified by Joshi et al. (2012) was applied to calculate the $Q_\beta(f)$ and source parameters. Kumar et al. (2015) studied shear wave attenuation by using the modified inversion of strong-motion data in the Kumaon Himalaya, India.

Several researchers have used different techniques to determine seismic attenuation in in the different part of Iran. For the East-Central Iran, Mahood and Hamzehloo (2009, 2011) and Mahood et al. (2009) estimated the coda wave attenuation and high frequency *P*- and *S*-waves attenuation, respectively. Motaghi and Ghods (2012) studied the attenuation of ground-motion spectral amplitudes and its variations across the central Alborz Mountains. Rahimi et al., (2010) and Farrokhi et al., (2015) estimated coda-wave attenuation in the central and eastern Alborz. Farrokhi and Hamzehloo (2016) investigated body wave attenuation characteristics in the Alborz region and north central Iran. In the NW-Iran, however, a few research has been performed. Zafarani et al., (2015) found the frequency-dependent S-wave quality factor, $Q_s=99f^{0.77}$ from the stochastic simulation of strong-motion records

[1]Assistant Professor, International Institute of Earthquake Engineering and Seismology (IIEES), Tehran, Iran, m.mahood@iiees.ac.ir

[2]Instructor, Department of civil engineering, Payam Noor University, PO BOX 19395-3697 Tehran, Iran. Shima.tahery@gmail.com.

of the Ahar-Varzaghan earthquakes.
This article uses data from the strong-motion network installed in the NW-Iran to study the seismicity and attenuation of shear waves in this region. We have used the vertical component of acceleration records, which is supposedly free from the site effects. Forty events recorded at 12 stations were utilized for the present work. The input parameters, such as seismic moment and corner frequency, are calculated from the inversion algorithm.

2. STUDY REGION AND DATA

The 6.4 M_w Ahar–Varzaghan (named after two nearby cities) earthquake occurred at 12:23 UTC on 2012 August 11 in East Azerbaijan province in northwestern Iran (Fig. 1). It was followed 11 min later by a second event of comparable size, 6.3 M_w. The comparable magnitudes of the two events and their close spatial and temporal relationship justify treating them as an earthquake doublet (Xu and Schwartz 1993). The doublet mainshocks were followed by three events of magnitude 5+ and many smaller aftershocks. The seismicity affected both the Varzaghan and Ahar regions and seriously damaged about 20 villages, killing 327 people and injuring more than 3000.
The region of NW-Iran is exceptional within the Arabian-Eurasian continental collision zone. The tectonics is dominated by the NW-SE striking right-lateral North Tabriz Fault (NTF), which is a major seismogenic fault in this region. Historical seismicity in the northwest of Iran is mostly associated with this Fault (Fig. 1). NW Iran is a region of intense deformation and seismicity situated between two thrust belts of the Caucasus to the north and the Zagros Mountains to the south (Hessami et al., 2003). Earthquake focal mechanisms suggest that the convergence between Arabia and Eurasia has been accommodated mainly through WNW-trending right-lateral strike-slip faults in this region. These strike-slip faults appear to be the southeastern continuation into NW-Iran of the North Anatolian Fault and other right-lateral faults in SE-Turkey. From paleoseismological observations conducted in several trenches cutting the fault at different places, Hessami et al. (2003) and Solaymani-Azad et al. (2011) concluded that the NTF experienced at least three strong earthquakes since 858 AD (Fig. 1). Last sequence of 3 events during the 18th century ruptured the total length of the NTF, and since that time, no large magnitude earthquake has been located on this fault (Moradi et al., 2011). The Ahar-Varzaghan doublet occurred in a region that has been characterized as having a low deformation rate and being bounded by deep-seated faults, among which the NTF is the most important (Hessami *et al.* 2003; Ghods *et al.* 2015; Donner *et al.* 2015).
Figure 1 shows an overview of northwestern Iran with topography, destructive and historical events (defined by date), location of the Ahar-Varzeghan earthquakes, focal mechanisms for both mainshocks and 5 aftershoks according to international agencies (CMT), strong-motion stations and active faults. The last damaging earthquakes on NTF occurred in 1721, rupturing the southeastern fault segment, and in 1780, rupturing the northwestern part. Tabriz, one of the major cities of NW-Iran, suffered major damage in both the 1721 and 1780 events.
The doublet mainshocks and various aftershocks used in the present study were recorded at different stations from 2012 August 11 to 2012 November 7. Location of mainshocks and 38 aftershoks used for Q_β estimation are shown in Figure 1. The strong ground motion network, installed by the Building and Housing Research Centre since 1972, includes 12 stations. All instruments were composed of SSA-2 digital accelerographs with a 10-Gal (0.1 m/s^2) threshold, sampling rate of 200 Hz, and natural frequency of 50 Hz.
These earthquakes were recorded in more than 50 strong-motion stations but we considered 40 accelerograms that have relatively strong signal to noise ratios (S/N>3) which enabled a relatively accurate determination of the source parameters and Q factor. The magnitudes of the aftershoks are from 4.1 to 5.5 and were recorded at distances of less than 100 km from the hypocenter.
Recorded waveforms were corrected for drift and baseline, and waveforms were low-pass filtered, with cutoff frequency at 25 Hz, and then vectorized and a time window containing the direct S-wave was selected from the accelerograms by using Kinoshita algorithm (1994). The displacement amplitude spectrum of each acceleration record, at each recording station, was computed by applying Fast Fourier Transform (FFT) to the corresponding time window, and the output of the Fourier transform was post-multiplied by ω^2 to obtain displacement spectrum (Figure 2 and 3).

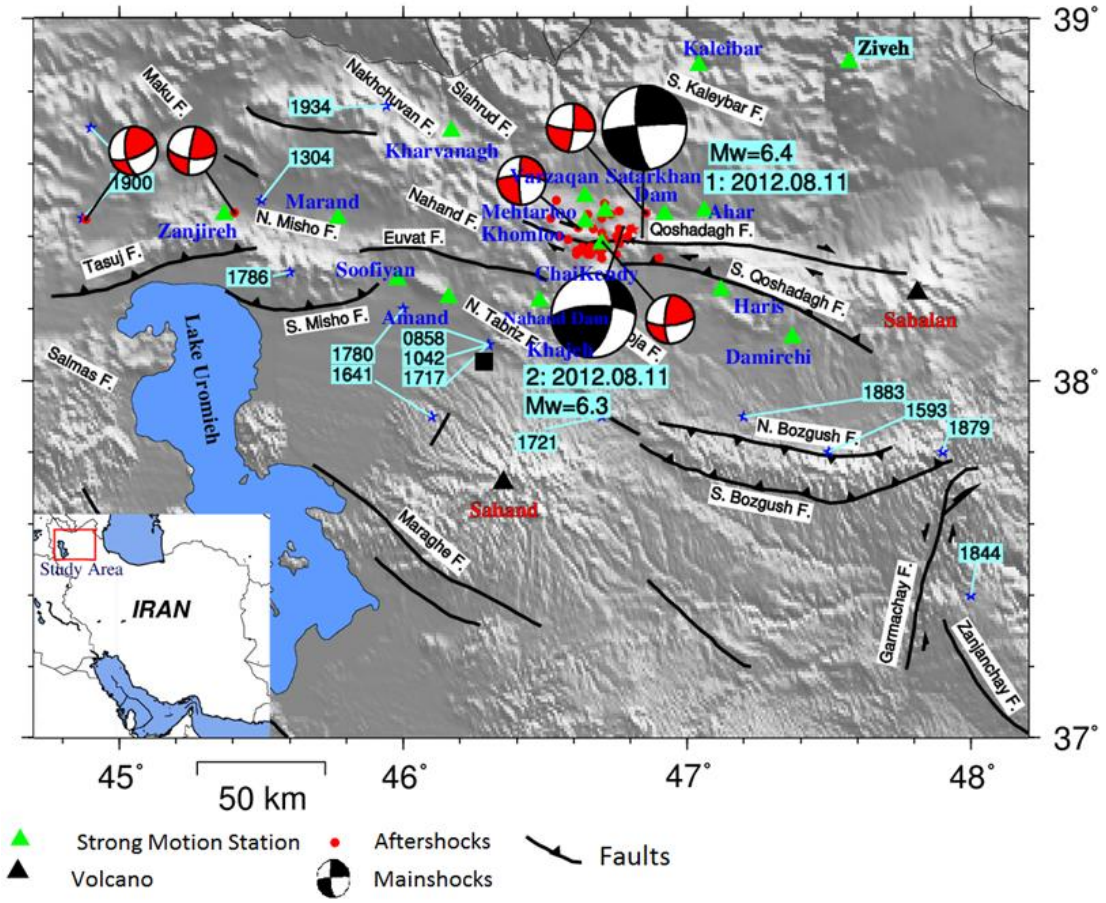

Figure 1. An overview of topography and historical events (by date) of NW-Iran with the Ahar-Varzeghan earthquakes and aftershocks (red circle), mechanisms for both mainshocks and 5 aftershoks, strong-motion stations (green triangles) and active faults.

3. INVERSION

Seismic moment is one of the most important parameters, which is required as an input to the present algorithm. This is computed from the source spectrum of the recorded data by using Brune's model (Brune, 1970). In this process, a time window of length covering the entire S-phase is applied to the corrected accelerogram. The sampled window is cosine tapered with 10% taper at both ends (Sharma and Wason, 1994). The spectrum of this time series is obtained by using a FFT algorithm and is then corrected for the anelastic attenuation and geometrical spreading terms. The plots of median source spectra of the events, as computed from the recorded data, are shown in Figures 3 and 4. By using the long-term flat levels in these spectra, the seismic moment of each event is calculated. Based on Brune's model (Brune, 1970), the seismic moment M_o of an earthquake can be calculated from the long-term flat level of the displacement spectrum given by

$$M_o = \frac{4\pi\rho\beta^3\Omega_o R}{R_{\theta\varphi}} \tag{1}$$

where ρ and β are the density and S-wave velocity of the medium, respectively, Ω_o is the long-term flat level of the source displacement spectrum at the hypocentral distance R, and $R_{\theta\varphi}$ is the radiation pattern coefficient. We use the density of medium as 2.8 g/cm^3 and shear wave velocity as 3.5 km/s (Zafarani *et al.* 2015), respectively. The fault plane solution for each event used in the present work could not be determined owing to the small number of recording stations. Therefore, the radiation

pattern term $R_{\theta\varphi}$ for S-wave is approximately taken as 0.55 (Atkinson and Boore, 1995). To estimate the moment magnitude using relation of Hanks and Kanamori (1979)

$$M_w = \frac{2}{3}\log(M_o) - 10.7 \tag{2}$$

The acceleration spectrum of shear waves at distance R due to an earthquake of seismic moment M_o can be given at frequency f as (Boore, 1983; Atkinson and Boore, 1998)

$$A(f) = CS(f, f_c)D(f) \tag{3}$$

where the term C is constant at a particular station for a given earthquake, $S(f, f_c)$ represents the source acceleration spectrum, and $D(f)$ denotes a frequency-dependent diminution function that takes into account the anelastic attenuation and attenuation due to geometrical spreading. This function modifies the spectral shape and is given as (Boore and Atkinson, 1987)

$$D(f) = \left[e^{(-\pi f R/Q(f)\beta)} G(R)\right] P(f, f_m) \tag{4}$$

$P(f,f_m)$ is a high-cut filter and $e^{(-\pi fR/Q(f)\beta)}G(R)$ is a propagation filter. $P(f,f_m)$ takes into account the fact that above some cutoff frequency (f_m), acceleration spectra show a sharp decrease (Boore, 1983). In the present work, we observed that above 25 Hz, the acceleration spectra decrease rapidly. Therefore, f_m is considered as 25 Hz in the analytical form of $P(f,f_m)$ given by Boore (1983). The term $e^{(-\pi fR/Q(f)\beta)}$ represents anelastic attenuation. In this term, $Q(f)$ is the frequency-dependent shear-wave quality factor, which needs to be determined. The function $G(R)$ represents the geometrical spreading term and is assumed to be equal to 1/R for R<100 km and equal to $1/(10R^{0.5})$ for R>100 km (Singh et al., 2006). As we are using the data from those events, which lie at the hypocentral distances ≤ 100 km, $G(R)$ is assumed as $1/R$. The geometrical factor term has been used as $1/R$ for the strong-motion studies of worldwide earthquakes by Boore (1983), Atkinson and Boore (1995), Joshi and Midorikawa (2004), Joshi (2006b) and Kumar et al. (2015).

For a double-couple seismic source embedded in an elastic medium, on considering only S-waves, C is a constant for a given station for a particular earthquake and is given as (Boore, 1983)

$$C = M_o R_{\theta\varphi}.FS.PRTITN / \left(4\pi\rho\beta^3\right) \tag{5}$$

in which M_o is the seismic moment, $R_{\theta\phi}$ is the radiation pattern, FS is the amplification due to the free surface, PRTITN is the reduction factor that accounts for partitioning of energy into two horizontal components, and ρ and β are the density and the shear-wave velocity, respectively. In the inversion procedure, the vertical component of a record is used to remove the possibility of site effects in the horizontal components. Therefore, in order to have consistency in the inversion procedure, source spectra are computed from the vertical components of records. For computing seismic moments in the inversion procedure from the vertical components, we do not include the term, which accounts for the division of energy into two horizontal components. It is also noticed that corner frequencies for the vertical and horizontal motions will not be same. In order to keep a consistency in the approach we compute source parameters from the vertical components and the same components are used for inversion. The $S(f, f_c)$ in Equation (3) defines the source spectrum of the earthquake. On using the spectral shape based on the ω^{-2} decay of high frequency proposed by Aki and Chouet (1975) and Brune (1970), $S(f, f_c)$is defined as

$$S(f, f_c) = \left(2\pi f\right)^2 / (1 + \left(f / f_c\right)^2) \tag{6}$$

Equation (3) serves as a foundation for the inversion algorithm. It should be linearized to determine the unknown parameter. Therefore, Equation (3) is linearized by taking its natural logarithm as

follows:

$$ln\ A(f) = ln\ C + ln\left(S(f, f_c)\right) - \pi f R / Q_\beta(f)\beta - ln(R) + lnP(f, f_m) \tag{7}$$

where $Q_\beta(f)$ and f_c are unknown. The term representing the source spectrum $S(f, f_c)$ can be replaced with the Equation (6). Further, with the assumption that f_c is known, the unknown parameter, $Q_\beta(f)$, can be obtained from the inversion by minimizing it in a least-squares sense. The least-squares inversion minimizes:

$$\chi^2 = \sum [A_s(f) - S(f, f_c)]^2 \tag{8}$$

where $S(f, f_c)$ is the theoretical source-acceleration spectrum and $A_s(f)$ is the source spectrum obtained from the record after substituting parameters $Q_\beta(f)$ obtained from the inversion. On rearranging the known and unknown quantities on different sides of equation (6) and substituting the term related to the source spectrum $S(f, f_c)$ as $(2\pi f)^2 / (1 + (f/f_c)^2)$, we obtain the following form:

$$-\pi f R / Q_\beta(f)\beta = ln\ A(f) - ln\ C - ln\left(2\pi f\right)^2 + ln[1 + (f / f_c)^2] + ln(R) - lnP(f, f_m) \tag{9}$$

In equation (9), the dependence on the corner frequency was linearized by expanding on $\ln(1+(f/f_c)^2)$ in a Taylor series around f_c. Accordingly, the following expression was obtained:

$$\begin{aligned} &-\pi f R / Q_\beta(f)\beta = ln\ A(f) - ln\ C - ln[(2\pi f)^2 / (1 + (f / f_c)^2)] \\ &-[2 / (1 + (f / f_c)^2)](f / f_c)^2 (\Delta f_c / f_c) + ln(R) - lnP(f, f_m) \end{aligned} \tag{10}$$

where Δf_c is the small change in the corner frequency and is an unknown quantity that is obtained from the inversion. In equation (10), the fourth term on the right side represents the Taylor series expansion of a fourth term in equation (9) as given by Fletcher (1995) and Joshi (2006a).
We obtained the following set of equations at a particular station for the ith earthquake for frequencies $f_1, f_2, f_3, \ldots, f_n$, where n denotes the total number of digitized samples in the acceleration record:

$$\begin{aligned} &-\pi f_1 R_{11} / Q_\beta(f_1)\beta + F(f_1 / f_{c1})\Delta f_c = D_{11}(f_1) \\ &-\pi f_2 R_{11} / Q_\beta(f_2)\beta + F(f_2 / f_{c1})\Delta f_c = D_{11}(f_2) \\ &. \\ &-\pi f_n R_{11} / Q_\beta(f_n)\beta + F(f_n / f_{c1})\Delta f_c = D_{11}(f_n) \end{aligned} \tag{11}$$

where $F(f_1,f_c)=[2/(1+(f_1/f_c)^2)](f_1/f_c)^2(1/f_c)$ is the term obtained from the expansion of $ln(1+(f/f_c)^2)$ in terms of a Taylor series around f_c. This function behaves linearly for known values of corner frequency f_c. For this reason, in the present work, f_c was used as an input parameter; its several possibilities were checked, and its final value was selected by minimizing the root mean square error (RMSE). For another station, the set of equations is

$$\begin{aligned} &-\pi f_1 R_{12} / Q_\beta(f_1)\beta + F(f_1 / f_{c1})\Delta f_c = D_{12}(f_1) \\ &-\pi f_2 R_{12} / Q_\beta(f_2)\beta + F(f_2 / f_{c1})\Delta f_c = D_{12}(f_2) \\ &. \\ &-\pi f_n R_{12} / Q_\beta(f_n)\beta + F(f_n / f_{c1})\Delta f_c = D_{12}(f_n) \end{aligned} \tag{12}$$

Subscripts i and j represent the event and the station number, respectively. Therefore, to generalize

equation (12), $D_{ij}(f_i)$ is given as

$$D_{ij}(f_i) = ln\ A_{ij}\left(f_{ij}\right) - ln\ C_i - ln[(2\pi f)^2 / (1+(f/f_{ci})^2)] + ln\left(R_{ij}\right) - lnP\left(f, f_m\right) \quad (13)$$

In the matrix form, this set of equations can be solved. The matrix can be represented in the following form:

$$Gm = d \quad (14)$$

Model parameters are contained in the model matrix *m* and the spectral component in the data matrix *d*. Inversion of the G matrix using Newton's method gives the model matrix m as

$$m = (G^T G)^{-1} G^T d \quad (15)$$

The inversion resulting in equation (15) is prone to problems if G^TG is even close to singular, and in such a case, singular value decomposition is used to solve equation (15) (Press et al., 1992).
The corner frequency is treated as the input parameter in the inversion algorithm to maintain the linearity in equation (13). We have used the solution that is obtained corresponding to minimum RMSE. In the present inversion scheme, several possibilities of corner frequencies are checked by iteratively changing the corner frequency f_c in an increment of Δf. The small increment Δf considered in the present work is 0.2 Hz.

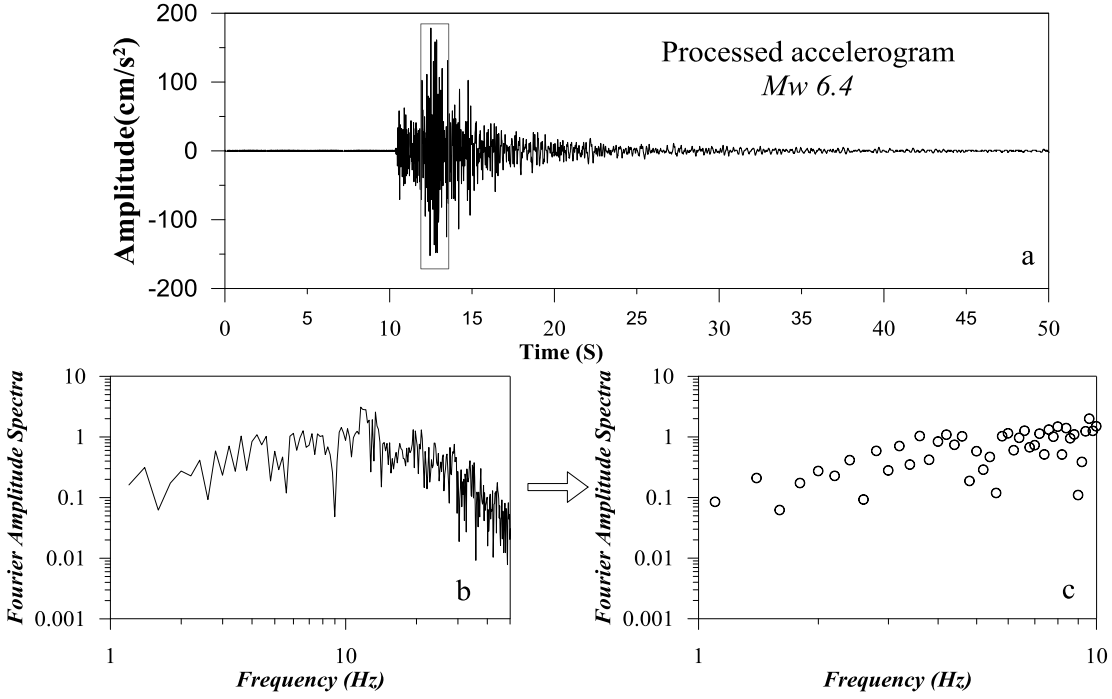

Figure 2. (a) Processed accelerogram at AHAR station; (b) Acceleration spectrum of S-phase marked by rectangular block with a time window of 4.0 s; (c) Discrete value of acceleration spectra used for present inversion (the discrete values of acceleration spectra are shown by small circles).

4. RESULTS AND DISCUSSION

In this research, source and path parameters are determined by using strong-motion data for 40 earthquakes recorded at the 12 stations in the study region. The advantage of using strong-motion data for the inversion is that it includes valuable high-frequency near-field data suitable for engineering use. The spectral parameters (M_o, f_c and Q_β) are estimated from the Brune's spectra after obtaining the

best fit between the observed and Brune's spectra, and the measure of best fit is represented in terms of minimizing errors in a least-squares sense.

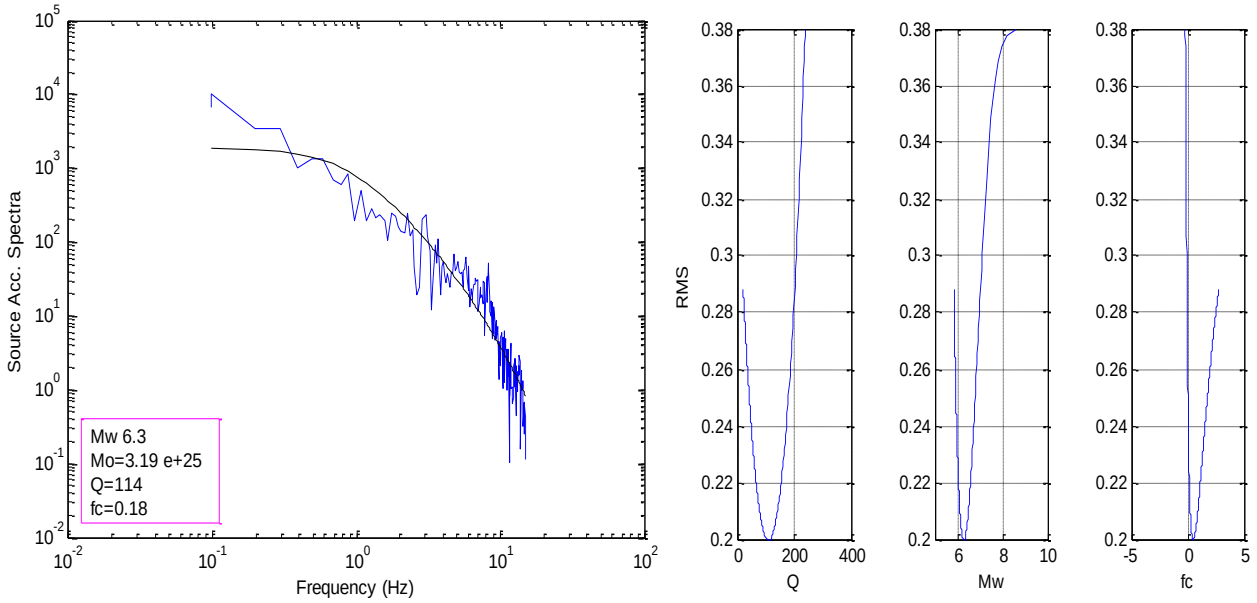

Figure 3. Left: The observed spectra and the fitted Brune source model. Right: the error values between theoretical and observed models for Q_β, M_w and f_c parameters.

The seismic moment of each event was determined using the source displacement spectra. Computed values of seismic moment at different stations were used to calculate the average seismic moment for each event. The RMS in the obtained and observed data was calculated for each case, and the solution corresponding to minimum RMS gave a direct estimate of $Q_\beta(f)$ together with the value of the corner frequency and seismic moment.

Figure 3 shows the observed spectra and a solid line which indicates the theoretical spectra of the Brune source model (left hand) for mainshock (M_w *6.4*) and the error values between theoretical and observed models for Q_β, M_w and f_c parameters (right hand). These parameters are estimated as Q_β=114, M_w 6.3 and f_c=0.18 Hz with minimum errors.

It is difficult to check which estimate of Q better describes the actual attenuation because there is no means of comparison directly or indirectly in earlier studies (Joshi, 2006a). This method has an advantage that the obtained $Q(f)$ values are checked by computing source spectra from the digital record at each station. The fit of observed spectra with a theoretical spectrum estimates the efficacy of our approach and reliability of the obtained $Q(f)$ relationship. Minimum error is obtained for the case of 4.0 s S-phase time window and that it increases when this window is either increased or decreased. This may be due to the overlapping of other phases in the input record for larger time windows and incomplete S-phases in smaller time windows (Joshi et al., 2010). Figure 4 shows an example of selected portions of the shear wave (4 s) and the source spectra of the first Ahar-Varzaghan earthquake (M_w *6.4*), as used for the inversion, and comparisons of the source spectra from the actual records and those from the Brune's model in 3 different stations; Soofian, Tabriz and Haris, respectively. Magnitude and Q_β are estimated as M_w *6.0, 6.3, 6.3* and Q_β*=103, 90* and *81* with minimum errors.

The average $Q(f)$ relation of form $Q_o f^{\,n}$ obtained by using average Q_β values obtained from inversion of records for the region stations are given in Table 1. The iterative inversion was performed at each station independently. It shows that the Q_β estimates vary for near and far stations from the mainshock epicenter. Lower Q_β values can be observed for near mainshock epicenter stations (i.e. Varzaghan, Q_o*=46*) and higher Q_β values for distant stations (i.e. Zanjireh, Q_o*=157*). The environment of the epicenter is more affected by the released energy and seismic waves recorded in the near field are propagated in the filled crack area.

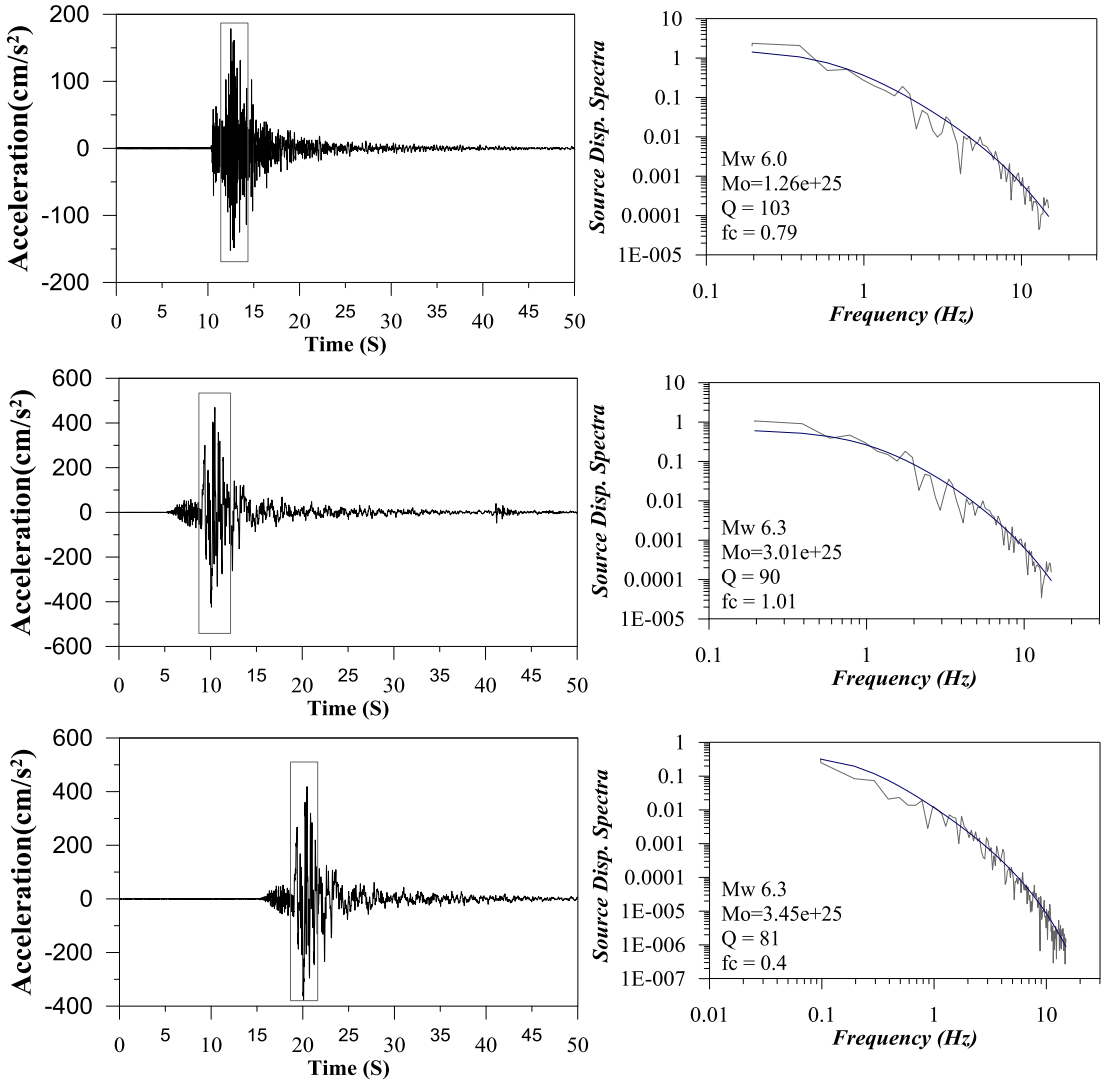

Figure 4. Selected portions of the vertical component of the accelerograms of the Ahar-Varzaghan earthquake, as used for the inversion, and comparisons of the source spectra from the actual records and those from the Brune's model (see the acceleration records at left hand in the Soofian, Tabriz and Haris stations, and the source spectra at the right hand); the thick solid line shows the theoretical Brune's spectrum, and the spectrum from the observed record is shown by the thin dark line.

A comparison of $Q_\beta(f)$ obtained from present study is made with the measurements of $Q_\beta(f)$ in other parts of the world in Figure 5. Measured Q_β values in the NW-Iran are in the range of seismically active regions such as Kumaon Hymalaya (Joshi *et al.* 2010). Figure 5 suggests that the NW-Iran falls in the seismotectonically active region. As Sharma *et al.* (2008) have noted, the area has a considerably thick layer of sediments due to which most of the energy gets dissipated into the medium.

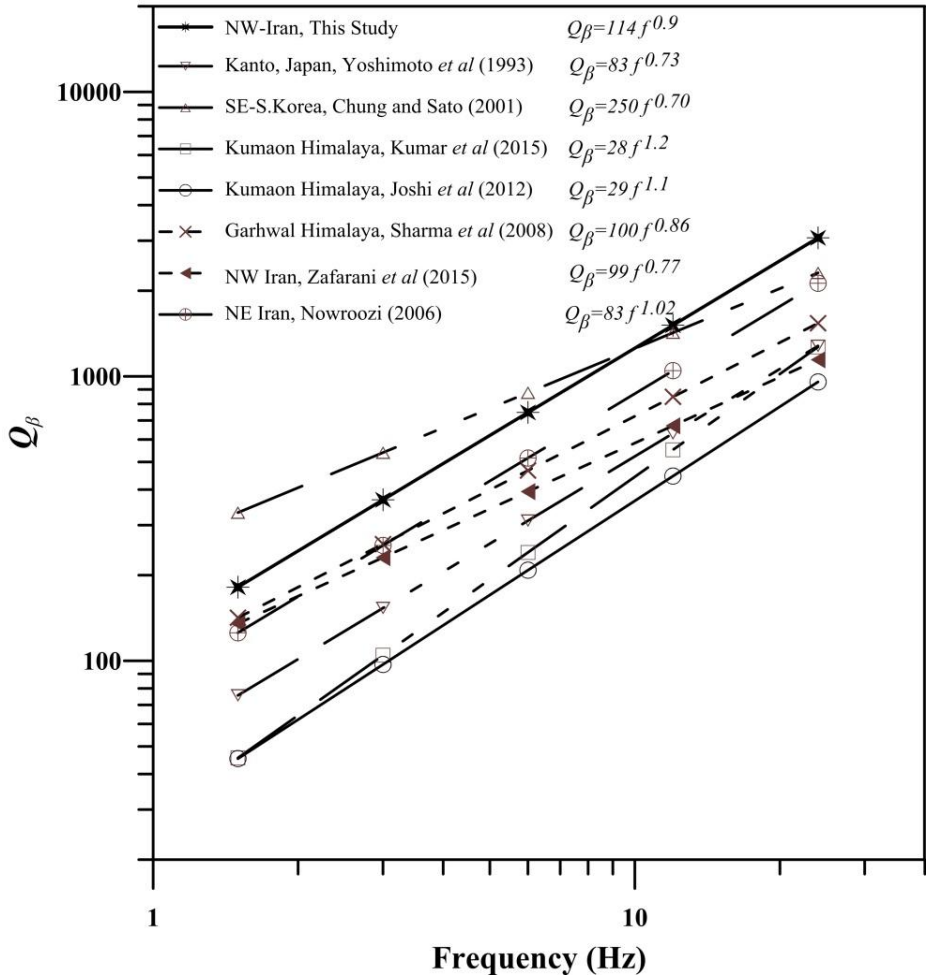

Figure 5. Comparison of $Q_\beta(f)$ relations developed in the present study with that obtained for worldwide region.

Table 1. The average values of the $Q_\beta(f)$ for the region stations.

Station	Q(f) Relation
Tabriz	$Q(f)=(92 \pm 13)\, f^{(0.76 \pm 0.09)}$
Chai Kendy	$Q(f)=(49 \pm 12)\, f^{(0.85 \pm 0.09)}$
Varzaqan	$Q(f)=(46 \pm 11)\, f^{(0.79 \pm 0.08)}$
Khajeh	$Q(f)=(77 \pm 19)\, f^{(0.78 \pm 0.07)}$
Khomloo	$Q(f)=(112 \pm 19)\, f^{(0.81 \pm 0.06)}$
Amand	$Q(f)=(96 \pm 21)\, f^{(0.82 \pm 0.07)}$
Kaleibar	$Q(f)=(52 \pm 16)\, f^{(0.92 \pm 0.08)}$
Soofiyan	$Q(f)=(110 \pm 21)\, f^{(0.74 \pm 0.08)}$
Damirchi	$Q(f)=(73 \pm 13)\, f^{(0.90 \pm 0.09)}$
Kharvanagh	$Q(f)=(140 \pm 19)\, f^{(0.69 \pm 0.09)}$
Ziveh	$Q(f)=(126 \pm 18)\, f^{(0.76 \pm 0.06)}$
Zanjireh	$Q(f)=(157 \pm 24)\, f^{(0.79 \pm 0.09)}$

5. CONCLUSIONS

In the present study, an inversion algorithm was performed to obtain the $Q_\beta(f)$ relationship and source parameters in the Ahar-Varzaghan region, NW-Iran, using strong-motion data. The minimum error is obtained in the inversion scheme for a relationship which gives $Q_\beta=(114\pm21)f^{(0.90\pm0.07)}$ for the study region, which represents the large heterogeneities and high level of tectonic activity of this region. The estimated relation indicates high attenuating crust beneath the source region, which makes this region seismically hazardous for future earthquakes, that requires special attention to determine its seismic hazard. The obtained $Q_\beta(f)$ is used to correct the spectrum and this corrected spectrum is further utilized to compute various parameters i.e. seismic moment and corner frequency. The best fit Brune's (1970) theoretical spectrum with the observed corrected spectrum provides these source parameters for the earthquakes of magnitude range 4.1 to 5.5 used in present work. The obtained values of M_o and f_c are 3.19×10^{25} dyne.cm and 0.69 Hz, respectively for the Ahar-Varzaghan first earthquake.

6. ACKNOWLEDGMENTS

The authors sincerely thank the International Institute of Earthquake Engineering and Seismology (IIEES) for supporting this research and providing the data. The authors also want to acknowledge Building and Housing Research Center (BHRC) for providing the data.

7. REFERENCES

Aki, K. and Chouet, B., 1975. Origin of Coda waves: Source, Attenuation and Scattering Effects, J. Geophys. Res 80, 3322–3342.

Atkinson, G. M., and D. M. Boore, 1995. Ground-motion relation for eastern North America, Bull. Seismol. Soc. Am. 85, 17–30.

Atkinson, G. M., and D. M. Boore, 1998. Evaluation of models for earthquake source spectra in eastern North America, Bull. Seism. Soc. Am. 88, 917–934.

Boore, D. M., 1983. Stochastic simulation of high-frequency ground motions based on seismological models of the radiated spectra, Bull. Seism. Soc. Am. 73, 1865–1894.

Boore, D. M., and G. M. Atkinson, 1987. Stochastic prediction of ground motion and spectral response parameters at hard-rock sites in eastern North America, Bull. Seism. Soc. Am. 77, 440–467.

Brune, J. M., 1970. Tectonic stress and spectra of seismic shear waves from earthquakes, J. Geophys. Res. 75, 4997–5009.

Donner, S., A. Ghods, F. Krüger, D. Robler, A. Landgraf and P. Ballato, 2015. The Ahar-Varzaghan Earthquake Doublet (Mw6.4 and 6.2) of 11 August 2012: Regional Seismic Moment Tensors. Bull Seismol. Soc. Am. 105(2A): 791 - 807.

Farrokhi, M., Hamzehloo, H., Rahimi, H., and Allameh Zadeh, M., 2015. Estimation of Coda-Wave Attenuation in the Central and Eastern Alborz, Iran, Bull. Seismol. Soc. Am. 105.

Farrokhi, M. and H., Hamzehloo, 2016. Body wave attenuation characteristics in the crust of Alborz region and North Central Iran, J. Seismol, 1–16.

Fletcher, J.B., 1995. Source parameters and crustal Q for four earthquakes in South Carolina, Seism. Res. Lett. 66, 44–58.

Ghods, A., Shabanian, E., Bergman, E., Faridi, M., Donner, S., Mortezanejad G. and A. Aziz-Zanjani, 2015. The Varzaghan–Ahar, Iran, Earthquake Doublet (Mw 6.4, 6.2): implications for the geodynamics of northwest Iran, Geophys. J. Int. 203, 522–540.

Hanks, T. C., and H. Kanamori, 1979. A moment magnitude scale, J. Geophys. Res. 84, 2348–2350.

Hessami, K., F. Jamali and H. Tabassi, 2003. Major Active Faults of Iran (map). Ministry of Science, Research and Technology, International Institute of Earthquake Engineering and Seismology.

Joshi, A., and Midorikawa, S., 2004. A simplified method for simulation of strong ground motion using rupture model of the earthquake source, Journal of Seismology 8, 467–484.

Joshi, A., 2006a. Use of acceleration spectra for determining the frequency dependent attenuation coefficient and source parameters, Bull. Seismol. Soc. Am. 96, 2165–2180.

Joshi, A., 2006b. Analysis of strong motion data of the Uttarkashi earthquake of 20th October 1991 and the Chamoli earthquake of 28th March 1999 for determining the mid crustal Q value and source parameters, J. Earthq. Technol. 43, 11–29.

Joshi, A. Mohanty, M., Bansal, A. R., Dimri, V. P., and Chadha, R. K., 2010. Use of spectral acceleration data for determination of three dimensional attenuation structure in the Pithoragarh region of Kumaon Himalaya, J Seismol 14: 247–272.

Joshi, A., P. Kumar, M. Mohanty, A. R. Bansal, V. P. Dimri, and R. K. Chadha, 2012. Determination of Qβ(f) at different places of Kumaon Himalaya from the inversion of spectral acceleration data, Pure Appl. Geophys. 169, 1821–1845.

Kinoshita, S., 1994. Frequency-dependent attenuation of shear waves in the crust of the southern Kanto area, Japan, Bull. seism. Soc. Am., 84, 1387–1396.

Kumar, P., Joshi, A., Sandeep, Kumar, A., and R. K. Chadha, 2015. Detailed Attenuation Study of Shear Waves in the Kumaon Himalaya, India, Using the Inversion of Strong-Motion Data. Bull. Seismol. Soc. Am, 105, 4.

Mahood, M., and H. Hamzehloo, 2009. Estimation of coda wave attenuation in east central Iran, J. Seismol. 13, 125–139.

Mahood, M., Hamzehloo, H., and G. J. Doloei, 2009. Attenuation of high frequency P and S waves in the crust of the East-Central Iran, Geophys. J. Int. 179, 3, 1669–1678.

Mahood, M., and H. Hamzehloo, 2011. Variation of intrinsic and scattering attenuation of seismic waves with depth in the Bam region, East-Central Iran, Soil Dynamics and Earthquake Engineering, 31, 1338–1346.

Mahood, M., 2014. Attenuation of high-frequency seismic waves in Eastern Iran. Pure Appl. Geophys., 171: 2225- 2240.

Moradi, S., D. Hatzfeld, and M. Tatar, 2011. Microseismicity and seismotectonics of the North Tabriz Fault (Iran), Tectonophysics 506, 22–30.

Motaghi, K., and Ghods, A., 2012. Attenuation of ground-motion spectral amplitudes and its variations across the central Alborz Mountains, Bull. Seismol. Soc. Am. 102, 1417–1428.

Press, W.H., Teukolsky, S.A., Vetterling, W.T. and Flannery, B.P., 1992. Numerical Recipes, Cambridge University Press, New York, U.S.A.

Rahimi, H., Motaghi, K., Mukhopadhyay, S., and Hamzehloo, H., 2010. Variation of coda wave attenuation in the Alborz region and central Iran, Geophys. J. Int. 181, 1643–1654.

Sato, H., Fehler, M. C. and Maeda, T., 2012. Seismic Wave Propagation and Scattering in the Heterogeneous Earth, Second Ed., Springer, New York, New York, 1-496.

Sharma, M. L., and H. R. Wason, 1994. Occurrence of low stress drop earthquakes in the Garhwal Himalaya region, Phys. Earth Planet. Int. 34, 159–172.

Sharma, B., Gupta, K.A., Devi, K.D., Kumar, D., Teotia S.S. and Rastogi, B.K., 2008. Attenuation of High-Frequency Seismic Waves in Kachch Region, Gujarat, India,. Bull. seism. Soc. Am., 98(5), 2325–2340.

Singh, S.K., Iglesias, A., Dattatrayam, R.S., Bansal, B.K., Rai, S.S., Perez-Campos, X., Suresh, G., Baidya, P.R. and Gautam, J.L., 2006. Muzaffarabad Earthquake of 8 October 2005 (7.6 Mw): A Preliminary Report on Source Characteristics and Recorded Ground Motions, Current Science, Vol. 91, No. 5, pp. 689–695.

Solaymani Azad, S., Dominguez, S., Philip, H., Hessami, K., Forutan, M.R., Shahpasan Zadeh, M. and Ritz, J.-F., 2011. The Zandjan fault system: Morphological and tectonic evidences of a new active fault network in the NW of Iran, Tectonophysics, 506, 73–85.

Zafarani, H., M. Rahimi, A. Noorzad, B. Hassani, B. Khazaei, 2015. Stochastic simulation of strongmotion records from the 2012 Ahar–Varzaghan Dual Earthquakes, Northwest of Iran. Bull. Seismol. Soc. Am., 105:1419 -1434.

Xu, Z. and S. Y. Schwartz, 1993. Large earthquake doublets and fault plane heterogeneity in the northern Solomon Islands subduction zone, pure and applied geophysics, V. 140, 2, 365-390.